

Convolutional Pose Machines

Shih-En Wei

shihenw@cmu.edu

Varun Ramakrishna

varunnr@cmu.edu

Takeo Kanade

Takeo.Kanade@cs.cmu.edu

Yaser Sheikh

yaser@cs.cmu.edu

The Robotics Institute
Carnegie Mellon University

Abstract

Pose Machines provide a powerful modular framework for articulated pose estimation. The sequential prediction framework allows for the learning of rich implicit spatial models, but currently relies on manually designed features for representing image and spatial context. In this work, we incorporate a convolutional network architecture into the pose machine framework allowing the learning of representations for both image and spatial context directly from data. The contribution of this paper is a systematic approach to composing convolutional networks with large receptive fields for pose estimation tasks. Our approach addresses the characteristic difficulty of vanishing gradients during training by providing a natural learning objective function that enforces intermediate supervision, thereby replenishing backpropagated gradients and conditioning the learning procedure. We demonstrate state-of-the-art performance and outperform competing methods on standard benchmarks.

1. Introduction

We introduce *Convolutional Pose Machines* for the task of articulated pose estimation. Convolutional pose machines inherit the benefits of the recently proposed *pose machine* [26] architecture—the implicit learning of long-range dependencies between image, multi-scale and multi-part cues, tight integration between learning and inference, a modular sequential design—and combine them with the advantages afforded by convolutional architectures: the ability to learn feature representations for both image and spatial context directly from data; a differentiable architecture that allows for all stages to be trained jointly with backpropagation; and the ability to efficiently handle large training datasets.

Convolutional pose machines consist of a sequence of prediction networks trained to predict confidences for the locations of each part, improving their predictions in each stage of the sequence (Figure 1). When convolutional networks are composed in such a way, it results in an overall

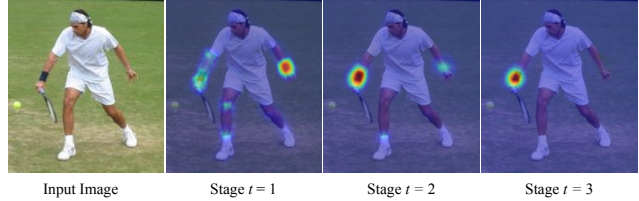


Figure 1: A Convolutional Pose Machine consists of a sequence of predictors trained to make a dense predictions at each image location. Here we show the increasingly refined estimates for the location of the *right wrist* in each stage of the sequence.

network with many layers that is at risk of the problem of *vanishing gradients* [4, 5, 9, 10] during learning. This problem can occur because backpropagated gradients diminish in strength as they are propagated through the many layers of the network. While there exists recent work which shows that supervising very deep networks at intermediate layers aids in learning [19, 33], they have mostly been restricted to simpler classification problems. In this work, we show how for a *structured prediction* problem such as pose estimation, Convolutional Pose Machines naturally suggest a systematic framework that replenishes gradients by enforcing intermediate supervision periodically through the network.

The design of the network in each stage of our sequential prediction framework is motivated by the goal of achieving a large receptive field on both the image and the output predictions of the preceding stage. We find, through experiment, that large receptive fields are crucial for learning long range spatial relationships and result in improved accuracy. Large receptive fields could be achieved by different designs: increasing pooling; increasing the number of layers; or increasing the kernel size of each convolutional filter. Each of these design choices come with trade-offs in either precision of localization, increase in network depth, or increase in parameters. We discuss the design of a convolutional architecture with intermediate supervision that achieves a large receptive field allowing for the encoding of long range spatial dependencies.

Our main contributions are (a) a sequential convolutional architecture that directly learns both image and image-dependent spatial context from data and (b) a systematic

approach to composing convolutional networks with large receptive fields for pose estimation tasks without the need for any graphical model style inference. We achieve state-of-the-art results on standard benchmarks, and analyze the effects of using an architecture with intermediate supervision, providing further evidence that networks with large depths can be effectively learned via intermediate supervision.

2. Related Work

The classical approach to articulated pose estimation is the **pictorial structures** model [2, 3, 8, 12, 24, 25, 27, 40] in which spatial correlations between parts of the body are expressed as a tree-structured graphical model with kinematic priors that couple connected limbs. These methods have been successful on images where all the limbs of the person are visible, but are prone to characteristic errors such as double-counting image evidence, which occur because of correlations between variables that are not captured by a tree-structured model. The work of Kiefel et al. [15] is based on the pictorial structures model but differs in the underlying graph representation. **Hierarchical models** [32, 34] represent the relationships between parts at different scales and sizes in a hierarchical tree structure. The underlying assumption of these models is that larger parts (that correspond to full limbs instead of joints) can often have discriminative image structure that can be easier to detect and consequently help reason about the location of smaller, harder-to-detect parts. **Non-tree models** [7, 14, 17, 30, 39] incorporate interactions that introduce loops to augment the tree structure with additional edges that capture symmetry, occlusion and long-range relationships. These methods usually have to rely on approximate inference during both learning and at test time. These methods usually have to trade off accurate modeling of spatial relationships with models that allow efficient inference and often require a simple parametric form to allow for fast inference. In contrast, methods based on a **sequential prediction** framework [26] learn an *implicit* spatial model with potentially complex interactions between variables by directly training an inference procedure as in [21, 23, 28, 38]. There has been a recent surge of interest in models that employ **deep convolutional architectures** for the task of articulated pose estimation [6, 22, 35, 36]. Tompson et al. [36] use a deep architecture with a graphical model whose parameters are learned jointly with the network. Toshev et al. [37] take the approach of directly regressing the full pose using a standard convolutional architecture [16].

In this work, we aim to combine the advantages of implicit spatial modeling via the sequential prediction framework of a pose machine [26] with recent advances in directly learning feature representations using deep convolutional architectures trained with backpropagation [16, 18]. We also leverage advances in developing fully convolutional deep architectures [20, 36] to achieve efficient dense pixel-wise predictions. Our resulting architecture can be

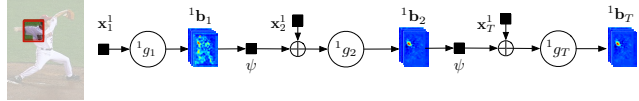


Figure 2: Pose Machines. A pose machine consists of a sequence of predictors that improve their predictions in each stage of the sequence using spatial context cues from the previous stage’s predictions.

viewed as a network with a large number of layers. Networks with many layers have been shown to be prone to the problem of *vanishing gradients*[4, 5, 9, 10] during training. While there has been some work examining architectures that bypass this problem [19, 31, 33] they have mostly been limited to classification problems. Most related is very recent work [19] where supervision is enforced after every layer of a deep network, which results in improved classification performance. In this work, we show how the sequential prediction framework of a pose machine forms the basis of a deep convolutional architecture that enforces intermediate local supervision. The intermediate supervision replenishes backpropagated gradients during training, and results in state-of-the-art performance on the structured prediction task of articulated pose estimation.

3. Method

3.1. Pose Machines

We denote the pixel location of the p 'th anatomical landmark (which we refer to as a part), $Y_p \in \mathcal{Z} \subset \mathbb{R}^2$, where \mathcal{Z} is the set of all (u, v) locations in an image. Our model consists of parts at different scales arranged in a hierarchy with *levels* $l \in \{1, \dots, L\}$. Our goal is to predict the image locations $Y = (Y_1, \dots, Y_{P_l})$ for all P_l parts in each of the L levels of the hierarchy. A pose machine [26] (see Figure 2) consists of a sequence of multi-class predictors, ${}^l g_t(\cdot)$, that are trained to predict the location of each part in each level of the hierarchy. In each *stage* $t \in \{1 \dots T\}$, the classifiers ${}^l g_t$ predict confidences for assigning a location to each part $Y_p = z$, $\forall z \in \mathcal{Z}$, based on features extracted from the image at the location z denoted by $\mathbf{x}_z \in \mathbb{R}^d$ and contextual information from the preceding classifier in the neighborhood around each Y_p . A classifier for the l 'th level of the hierarchy in the first stage $t = 1$, therefore produces the following confidence values:

$${}^l g_1(\mathbf{x}_z^l) \rightarrow \{{}^l b_1^p(Y_p = z)\}_{p \in \{0 \dots P_l\}}, \quad (1)$$

where ${}^l b_1^p(Y_p = z)$ is the score predicted by the classifier ${}^l g_1$ for assigning the p 'th part in the l 'th level of the hierarchy in the first stage at image location z . We represent all the confidences, or *beliefs*, of part p of level l evaluated at every location $z = (u, v)^T$ in the image as ${}^l \mathbf{b}_t^p \in \mathbb{R}^{w \times h}$, where w and h are the width and height of the image, respectively. That is,

$${}^l \mathbf{b}_t^p[u, v] = {}^l b_1^p(Y_p = z). \quad (2)$$

For convenience, we denote the collection of confidence

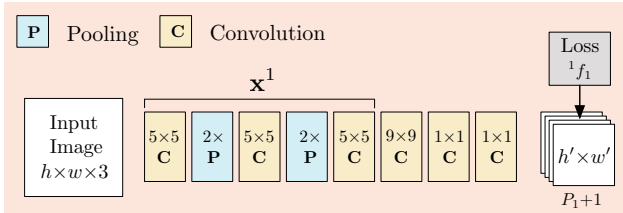


Figure 3: Convolutional Architecture for Keypoint Localization. We show a deep convolutional architecture for performing keypoint localization that relies on local image evidence in a small region (receptive field) around each pixel location.

maps for all the parts belonging to level l as ${}^l\mathbf{b}_t \in \mathbb{R}^{w \times h \times (P_l + 1)}$ (see Figure 7).

In subsequent stages, the classifier predicts a confidence for assigning a location to each part $Y_p = z$, $\forall z \in \mathcal{Z}$, based on (1) features of the image data $\mathbf{x}_z \in \mathbb{R}^d$ and (2) contextual information from the preceding classifier in the neighborhood around each Y_p :

$${}^l g_t \left(\mathbf{x}_z^l, \bigoplus_{l \in \{1 \dots L\}} \psi(z, {}^l \mathbf{b}_{t-1}) \right) \rightarrow \{{}^l b_t^p(Y_p = z)\}_{p \in \{0 \dots P_l\}}, \quad (3)$$

where \bigoplus denotes vector concatenation and $\psi(\cdot)$ is a mapping from the confidences \mathbf{b}_{t-1} to context features. In each stage, the computed confidences provide an increasingly refined estimate for the location of each part. The pose machine proposed in [26] used boosted random forests for prediction ($\{{}^l g_t\}$) and hand-crafted context feature maps ($\psi(\cdot)$) to capture spatial context.

3.2. Convolutional Pose Machines

We show how the prediction and image feature computation modules of a pose machine can be replaced by a deep convolutional architecture allowing for both image and contextual feature representations to be learned directly from data. Convolutional architectures also have the advantage of being completely differentiable, thereby enabling end-to-end joint training of all stages of a pose machine. We describe our design for a convolutional pose machine that combines the advantages of deep convolutional architectures with the implicit spatial modeling afforded by the pose machine framework.

3.2.1 Keypoint Localization Using Local Image Evidence

The first stage of a convolutional pose machine predicts part confidences from only local image evidence. Figure 3 shows the network structure used for part detection from local image evidence using a deep convolutional network. The evidence is *local* because the receptive field of the network is constrained to a tightly cropped patch around the keypoint location. We use a network structure composed of 6 convolutional layers followed by two 1×1 convolutional layers which results in a fully convolutional architec-

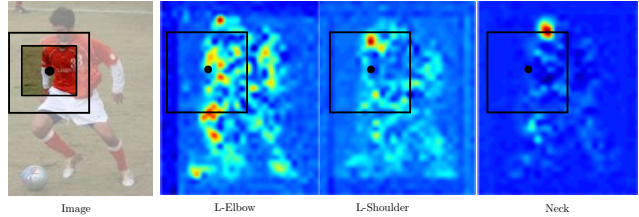


Figure 4: Spatial context from confidence maps can provide valuable cues for detection. The peaks in the confidence map for easier to detect landmarks, such as the shoulder, can be a strong cue for the location of difficult to detect landmarks, such as the left elbow.

ture [20] (see Figure 3) that allows inputs of an arbitrary size $w \times h$. The receptive field of the network shown above is 64×64 pixels. The network can effectively be viewed as sliding a deep network across an image and regressing from the local image evidence in each 64×64 image patch to a $P_1 + 1$ (plus one for background) sized output vector that represents a score for each part at that image location.

3.2.2 Sequential Prediction with Learned Spatial Context Features

While the detection rate on landmarks with consistent appearance, such as the head and shoulders, can be favorable, the accuracies can be much lower for landmarks lower down the kinematic chain of the human skeleton due to their large variance in configuration and appearance. The landscape of the confidence maps around a part location, albeit noisy, can, however, be very informative. The fact that the confidence map for the shoulder has a sharp peak in the vicinity of the elbow can be used as a strong cue for predicting the location of the elbow (see Figure 4). A predictor in subsequent stages (g_{t+1}) can use the spatial context ($\psi(\cdot)$) of the noisy confidence maps in a region around the image location z and improve its predictions by leveraging the fact that parts occur in consistent geometric configurations. In the second stage of a pose machine, the classifier ${}^l g_2$ accepts as input the image features \mathbf{x}_z^l and features computed on the confidences via the feature function ψ for each of the parts in the previous stage. The feature function ψ serves to encode the landscape of the confidence maps from the previous stage in a spatial region around the location z of the different parts. For a convolutional pose machine, we do not have an explicit function that computes context features. Instead, we define ψ as being the receptive field of the predictor on the confidences from the previous stage.

The design of the network is guided by achieving a receptive field at the output layer of the second stage network that meets that allows the learning of potentially complex and long-range correlations between parts by simply supplying features on the outputs of the previous stage (as opposed to specifying potential functions in a graphical model) and allowing the classifier to freely combine contextual information by picking the most predictive features. The confidence maps from the first stage are generated from a network that examined the image locally with a receptive

Convolutional Architecture for a 2-Stage Pose Machine

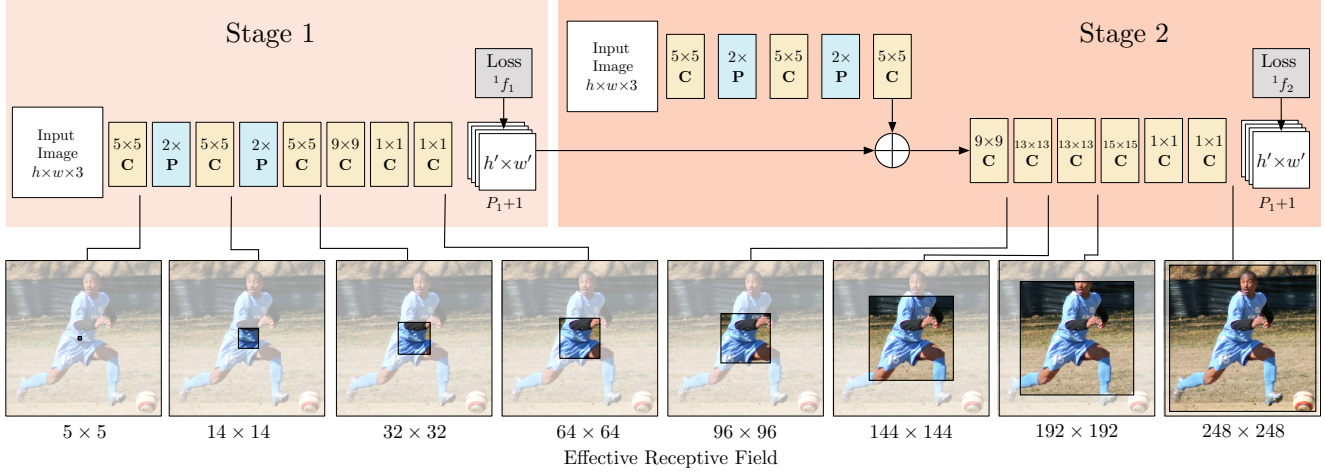


Figure 5: Convolutional Architecture for a 2-stage Pose Machine. We show a deep convolutional architecture for a pose machine with two stages. In the second stage we use a convolutional architecture that uses both confidence maps from the previous stage as well as features learned directly from the image. Below, we also show the effective receptive field on an image at various parts of the architecture.

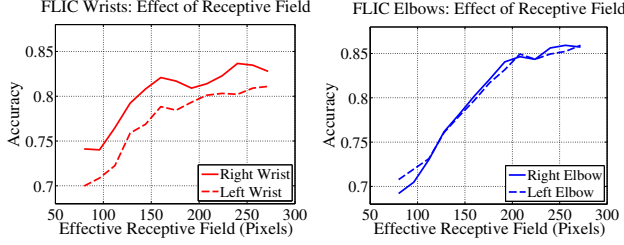


Figure 6: Large receptive fields for spatial context. We show that networks with large receptive fields are effective at modeling long range spatial interactions between parts.

field of size 64×64 . In the second stage, we design a network that drastically increases the equivalent receptive field. Large receptive fields can be achieved either by pooling at the expense of precision, increasing the kernel size of the convolutional filters at the expense of increasing the number of parameters, or by increasing the number of convolutional layers at the risk of encountering vanishing gradients during training. Our design for the two stage network is shown in figure 5. We choose to use multiple convolutional layers as it allows us to be parsimonious with respect to the number of parameters of the model while the risk of vanishing gradients is offset thanks to the intermediate supervision enforced during training.

We find that accuracy improves with the size of the receptive field. In Figure 6 we show the improvement in accuracy on the FLIC dataset [29] as the size of the receptive field on the original image is varied by varying the architecture. The two stage convolutional pose machine uses a combination of image feature maps and confidence maps passed as input to a network with four convolutional layers. The receptive field on the confidence maps of the first stage is 47×47 , which is equivalently 248×248 pixels on the original image. We see that the network achieves the best

accuracy at an effective receptive field of between $200 - 250$ which also happens to be roughly the size of the object in the normalized training images. This improvement in accuracy with receptive field size also suggests that the network does indeed encode long range interactions between parts and that doing so is beneficial.

3.2.3 Incorporating a Hierarchy

The visual structure around each landmark can provide discriminative information that is useful for prediction. Often-times larger regions around a landmark can contain more discriminative structure than a smaller, tightly cropped region. For example, for landmarks such as the wrist joint, a patch tightly cropped around it has little distinguishable visual structure. Whereas, when we include additional visual context, we observe the consistent discriminative visual structure of the forearm. Multi-scale cues such as these can be useful for detection. Pose machines incorporate such multiscale cues by defining a hierarchy over parts. The design of a convolutional pose machine that incorporates hierarchical cues across multiple stages is shown in 7. In stages after the first stage, the image feature maps (denoted by x_z^l) are combined with the confidence maps for the parts from both hierarchy levels from the previous stage. The confidence maps from preceding layers that are at a different resolution are correspondingly up-sampled using a deconvolutional layer [20] or down-sampled using a max-pooling layer of the appropriate stride.

3.3. Learning in Convolutional Pose Machines

The design described above for a pose machine results in a deep architecture that can have a large number of layers. Training such a network with many layers can be prone to the problem of *vanishing gradients* [4, 5, 9] where, as ob-

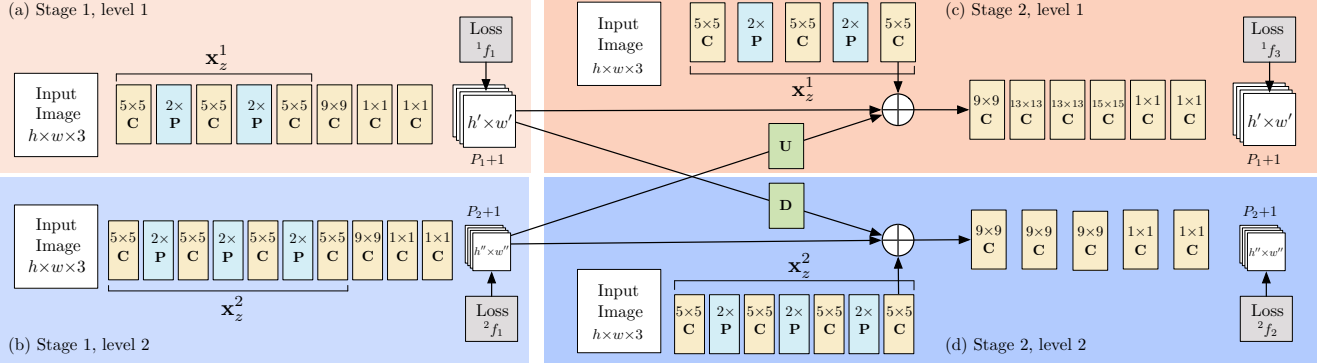
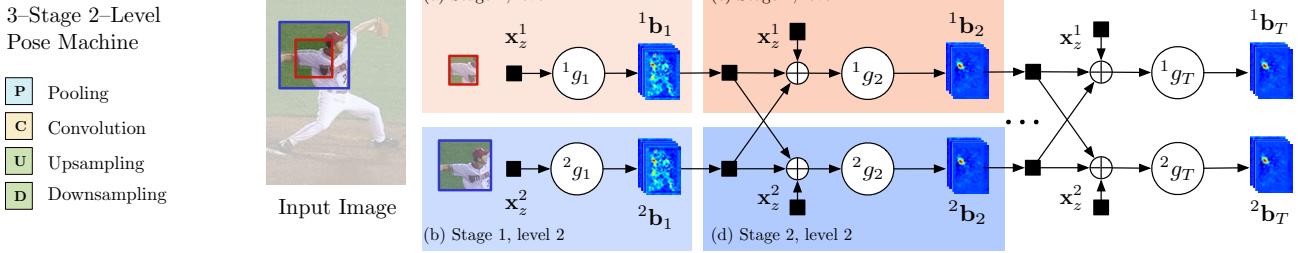


Figure 7: Architecture for Convolutional Pose Machines. We show a deep convolutional architecture for a pose machine with three stages and a two level hierarchy. The pose machine is shown in the top right with insets described below. Insets (a) and (b) show the architecture that operates only on image evidence in the first stage for each of the hierarchy levels. Insets (c) and (d) show the architecture for subsequent stages, which operate both on image evidence as well as confidence maps from preceding stages. The architectures in (c) and (d) are repeated for all subsequent stages. The network is locally supervised after each stage using an intermediate loss layer that prevents vanishing gradients during training. (Best viewed in color.)

served by Bradley [5] and Bengio et al. [9], the magnitude of backpropagated gradients decreases in strength with the number of intermediate layers between the output layer and the input layer.

Fortunately, the sequential prediction framework of the pose machine provides a natural approach to training our deep architecture that addresses this problem. Each stage of the pose machine is trained to repeatedly produce the confidence maps or *beliefs* for the locations of each of the parts. We encourage the network to repeatedly arrive at such a representation by defining a loss function at the output of each stage t and hierarchy level l that minimizes the l_2 distance between the predicted and ideal confidence maps for each part. The ideal confidence map for a part p is written as ${}^l b_*^p(Y_p = z)$. The cost function we aim to minimize at the output of each stage at each level is therefore given by:

$${}^l f_t = \sum_{p=1}^{P_l} \sum_{z \in \mathcal{Z}} \| {}^l b_t^p(z) - {}^l b_*^p(z) \|_2^2. \quad (4)$$

The overall objective for the full architecture is obtained by adding the losses at each stage and is given by:

$$\mathcal{F} = \sum_{t=1}^T \sum_{l=1}^L {}^l f_t. \quad (5)$$

Implementation Details: We define and implement our model using the *Caffe* [11] libraries for deep learning. We

will publicly release the source code and details on the architecture, learning parameters, design decisions and data augmentation to ensure full reproducibility.

4. Evaluation

4.1. Analysis

Addressing vanishing gradients. The objective in Equation 5 describes a decomposable loss function that operates on different parts of the network (see Figure 7). Specifically, each term in the summation is applied to the network after each stage t effectively enforcing supervision in intermediate stages through the network. Intermediate supervision has the advantage that, even though the full architecture can have many layers, it does not fall prey to the *vanishing gradient* problem as the intermediate loss functions replenish the gradients at each stage.

We verify this claim by observing histograms of gradient magnitude (see Figure 9) at different depths in the architecture across training epochs for models with and without intermediate supervision. In early epochs, as we move from the output layer to the input layer, we observe on the model *without intermediate supervision*, the gradient distribution is tightly peaked around zero because of vanishing gradients. The model *with intermediate supervision* has a much larger variance across all the layers, suggesting that learning is indeed occurring in all the layers thanks to intermediate supervision. We also notice that as training progresses, the variance in the gradient magnitude distributions decreases

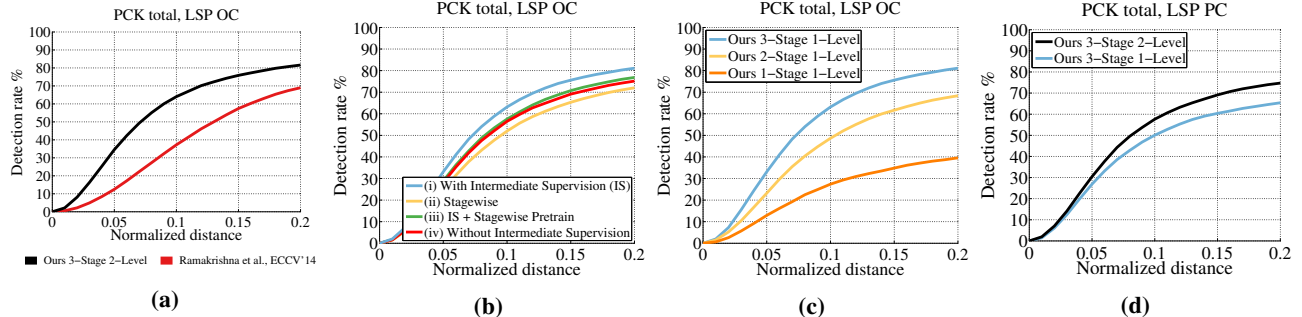


Figure 8: (a) Improvement over the Pose Machine proposed in [26] (b) Comparisons on the LSP dataset between the different training methods. (c) Comparisons on the LSP dataset across each stage using joint training from scratch with intermediate supervision. (d) Comparisons on the LSP dataset across number of stages using training from scratch with PC annotation.

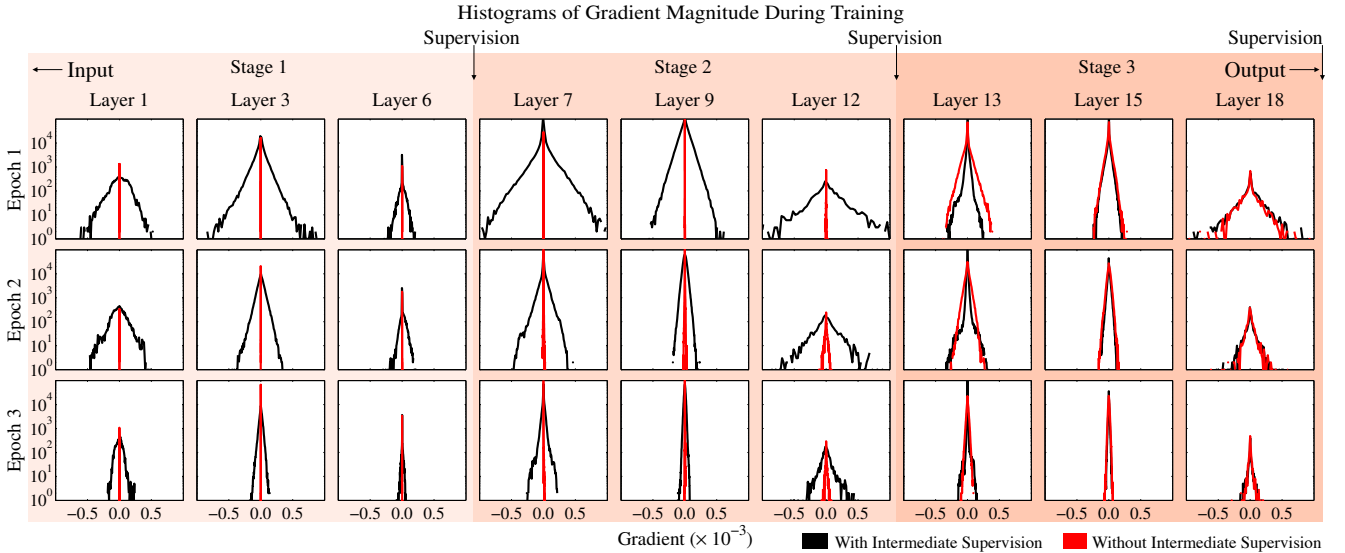


Figure 9: Intermediate supervision addresses vanishing gradients. We track the change in magnitude of weights in layers at different depths in the architecture, across training epochs, for models with and without intermediate supervision. We observe that for layers closer to the output the distribution has a large variance for both with and without intermediate supervision, however as we move from the output layer towards the input, the gradient magnitude distribution peaks tightly around zero with low variance (the gradients *vanish*) for the model without intermediate supervision. For the model with intermediate supervision the distribution has a moderately large variance throughout the network. At later training epochs, the variances decrease for all layers for the model with intermediate supervision and remain tightly peaked around zero for the model without intermediate supervision. (Best viewed in color)

pointing to model convergence.

Which learning method? We compare different variants of training the network in Figure 8b and demonstrate the benefit of intermediate supervision with joint training across stages using a model trained in four ways: (i) using a global loss function that enforces intermediate supervision (ii) stage-wise; where each stage is trained in a feed-forward fashion and stacked (iii) as same as (i) but initialized with weights from (ii), and (iv) as same as (i) but with no intermediate supervision. We find that network (i) outperforms all other training methods, showing that intermediate supervision and joint training across stage is indeed crucial in achieving good performance.

Benefit of end-to-end learning. We see in Figure 8a that replacing the modules of a pose machine with the appropriately designed convolutional architecture provides a large boost of close to 20 percentage points over the previous

approach of [26] in the high precision regime (PCK@0.1) and around 10 percentage points in the low precision regime (PCK@0.2).

Performance across stages. We show a comparison of performance across each stage on the LSP dataset in Figure 8c. We show that the performance increases monotonically across stages, as the predictors in subsequent stages make use of contextual information in a large receptive field on the previous stage confidence maps to resolve confusions between parts and background.

Does the hierarchy help? We compare models with one and two levels in the hierarchy on LSP in Figure 8d. We see a substantial improvement in performance with the two-level model when using person-centric (PC) annotations. The difficulty in learning person-centric pose estimation lies in the fact that the front-back ambiguity needs to be resolved. The favorable performance of the two-level model

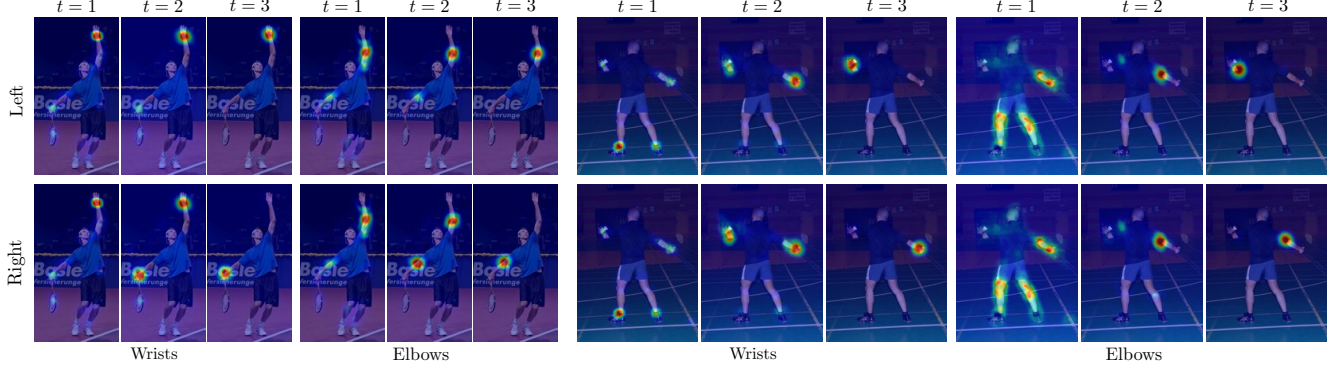


Figure 10: Comparison of confidence maps across stages for the elbow and wrist joints on the LSP dataset for a three stage deep pose machine. The subsequent stages of the convolutional pose machine learn a spatial model that aids in resolving confusions between parts. The first stage predictions for the wrist joints are often ambiguous or erroneous.

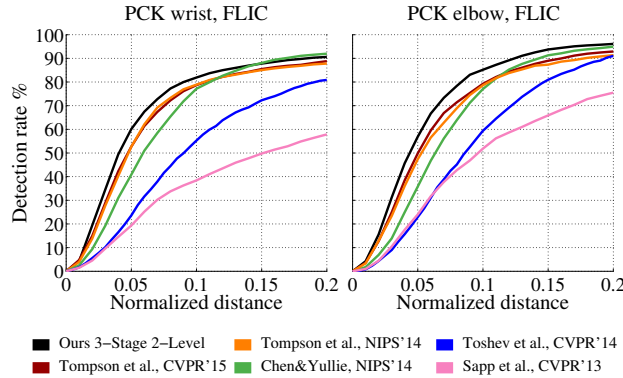


Figure 11: Quantitative results for the elbow and wrist joints on the FLIC dataset for a convolutional pose machine with three stages and two levels. We outperform all competing methods.

over the single-level model seems to suggest that information at a coarser scale assists the model in resolving this ambiguity.

4.2. Datasets and Quantitative Analysis

MPII Human Pose Dataset. We show in Figure 12 our results on the MPII Human Pose dataset [1] which consists more than 29000 training samples. The evaluation is based on PCKh metric [1] where the error tolerance is normalized with respect to head size of the target. Our total PCKh-0.5 score achieves state of the art at 87.95%, and it is noteworthy that on the ankle (the most challenging part), our PCKh-0.5 score is 78.28%, which is significantly better than all the competing methods. Our method improves the accuracy in all parts and over all precisions, and is the first one achieving such high accuracy without any pre-training from other data, or post-inference parsing (e.g., using a graphical model), which often needs prior knowledge of such a structured prediction task as in [35, 36].

Leeds Sports Pose (LSP) Dataset. We evaluate our method on the Extended Leeds Sports Dataset [13] that consists of 11000 images for training and 1000 images for testing. We trained two models each for both observer-

centric (OC) annotations and person-centric (PC) annotations respectively. We evaluate our method on both OC and PC annotations using the Percentage Correct Keypoints (PCK) metric [41]. We see that for *observer-centric annotations* (see Figure 13) we outperform the nearest competing method by approximately 10 percentage points in the high precision regime (PCK@0.1) and approximately 5 percentage points in the lower precision regime (PCK@0.2). *Person-centric annotations* impose a harder problem on the pose estimation task since disambiguating the left from right limbs relies on observing the target’s pose relative to the camera, in addition to the spatial relationship of parts in the image plane. Figure 10 shows that our model develops a representation that is able to resolve the left-right ambiguity across the stages with large receptive fields. Our method again outperforms all of the other methods, as shown in Figure 13.

FLIC Dataset. We evaluate our method on the FLIC Dataset [29] which consists of 3987 images for training and 1016 images for testing. We report accuracy as per the metric introduced in Sapp et al. [29] for the elbow and wrist joints in Figure 11. Again, we outperform all prior art in PCK metric in both high precision (PCK@0.05) by 7.5 percentage points on wrists and 7 percentage points on elbows, and in the lower precision regime (PCK@0.1) by 3 percentage points on wrists and 6.5 percentage points on elbows.

5. Discussion

The sequential prediction framework of pose machines provides a systematic framework to compose deep architectures for pose estimation. The training procedure describes a natural objective for learning a deep architecture with many layers by enforcing intermediate supervision addressing the *vanishing gradient* problem. Some failure cases include examples with rare poses, multiple people in close proximity and heavy occlusions. The model allows for making dense predictions that leverage semantic spatial context and future work would explore application in problem domains such as semantic segmentation and depth prediction.

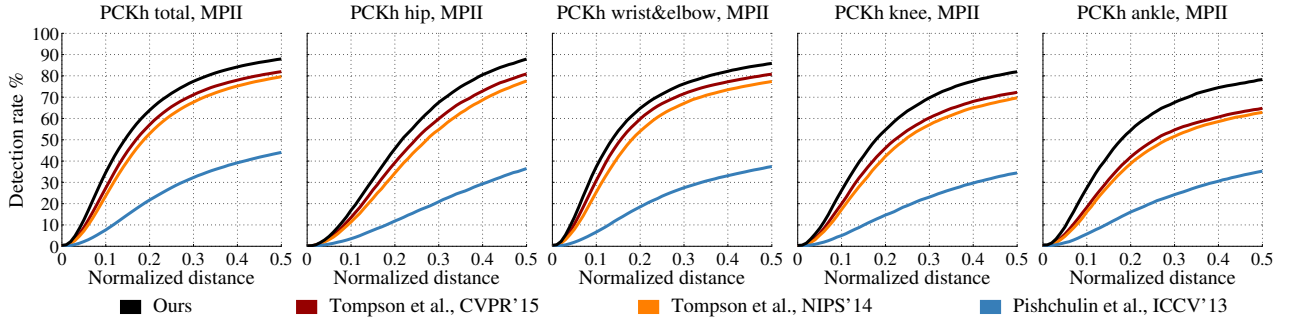


Figure 12: Quantitative results on the MPII dataset using the PCKh metric. We achieve state of the art and outperform significantly on difficult parts such as the ankle.

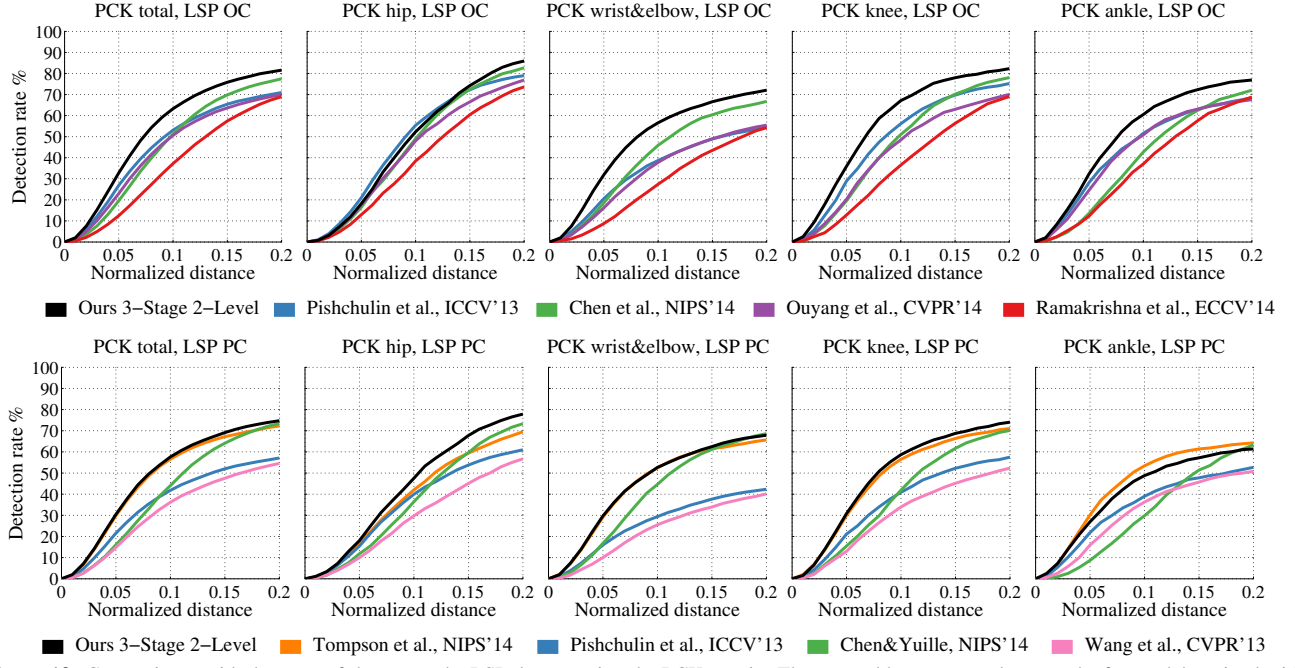


Figure 13: Comparisons with the state-of-the-art on the LSP dataset using the PCK metric. The top and bottom row show results for models trained with observer-centric and person-centric annotations respectively.

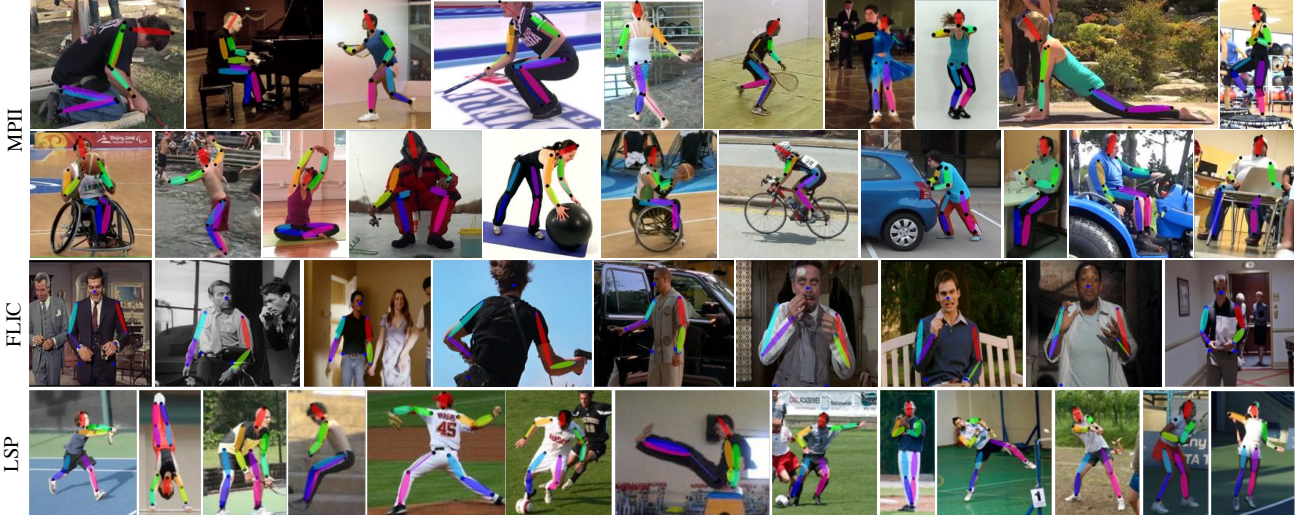


Figure 14: Qualitative results of our method on the MPII, LSP and FLIC datasets respectively. We see that the method is able to handle non-standard poses and resolve ambiguities between symmetric parts for a variety of different relative camera views.

References

- [1] M. Andriluka, L. Pishchulin, P. Gehler, and B. Schiele. 2d human pose estimation: New benchmark and state of the art analysis. In *CVPR*, June 2014. [7](#)
- [2] M. Andriluka, S. Roth, and B. Schiele. Pictorial Structures Revisited: People Detection and Articulated Pose Estimation. In *CVPR*, 2009. [2](#)
- [3] M. Andriluka, S. Roth, and B. Schiele. Monocular 3D Pose Estimation and Tracking by Detection. In *CVPR*, 2010. [2](#)
- [4] Y. Bengio, P. Simard, and P. Frasconi. Learning long-term dependencies with gradient descent is difficult. *Neural Networks, IEEE Transactions on*, 1994. [1, 2, 4](#)
- [5] D. Bradley . *Learning In Modular Systems*. PhD thesis, Robotics Institute, Carnegie Mellon University, Pittsburgh, PA, 2010. [1, 2, 4, 5](#)
- [6] X. Chen and A. Yuille. Articulated pose estimation by a graphical model with image dependent pairwise relations. In *NIPS*, 2014. [2](#)
- [7] M. Dantone, J. Gall, C. Leistner, and L. Van Gool. Human pose estimation using body parts dependent joint regressors. In *CVPR*, 2013. [2](#)
- [8] P. F. Felzenszwalb and D. P. Huttenlocher. Pictorial structures for object recognition. *IJCV*, 2005. [2](#)
- [9] X. Glorot and Y. Bengio. Understanding the difficulty of training deep feedforward neural networks. In *AISTATS*, 2010. [1, 2, 4, 5](#)
- [10] S. Hochreiter, Y. Bengio, P. Frasconi, and J. Schmidhuber. Gradient flow in recurrent nets: the difficulty of learning long-term dependencies, 2001. [1, 2](#)
- [11] Y. Jia, E. Shelhamer, J. Donahue, S. Karayev, J. Long, R. Girshick, S. Guadarrama, and T. Darrell. Caffe: Convolutional architecture for fast feature embedding. *arXiv preprint arXiv:1408.5093*, 2014. [5](#)
- [12] S. Johnson and M. Everingham. Clustered pose and non-linear appearance models for human pose estimation. In *BMVC*, 2010. [2](#)
- [13] S. Johnson and M. Everingham. Learning effective human pose estimation from inaccurate annotation. In *Proceedings of IEEE Conference on Computer Vision and Pattern Recognition*, 2011. [7](#)
- [14] L. Karlinsky and S. Ullman. Using linking features in learning non-parametric part models. In *ECCV*, 2012. [2](#)
- [15] M. Kiefel and P. V. Gehler. Human pose estimation with fields of parts. In *ECCV*. 2014. [2](#)
- [16] A. Krizhevsky, I. Sutskever, and G. E. Hinton. Imagenet classification with deep convolutional neural networks. In *NIPS*, 2012. [2](#)
- [17] X. Lan and D. P. Huttenlocher. Beyond trees: Common-factor models for 2d human pose recovery. In *ICCV*, 2005. [2](#)
- [18] Y. LeCun, B. Boser, J. S. Denker, D. Henderson, R. E. Howard, W. Hubbard, and L. D. Jackel. Backpropagation applied to handwritten zip code recognition. *Neural computation*, 1989. [2](#)
- [19] C.-Y. Lee, S. Xie, P. Gallagher, Z. Zhang, and Z. Tu. Deeply-supervised nets. *AISTATS*, 2015. [1, 2](#)
- [20] J. Long, E. Shelhamer, and T. Darrell. Fully convolutional networks for semantic segmentation. *CVPR*, 2015. [2, 3, 4](#)
- [21] D. Munoz, J. A. Bagnell, and M. Hebert. Stacked hierarchical labeling. In *ECCV*, 2010. [2](#)
- [22] W. Ouyang, X. Chu, and X. Wang. Multi-source deep learning for human pose estimation. In *CVPR*. IEEE, 2014. [2](#)
- [23] P. H. O. Pinheiro, R. Collobert, P. H. O. Pinheiro, and R. Collobert. Recurrent convolutional neural networks for scene labeling. In *International Conference on Machine Learning (ICML)*, 2014. [2](#)
- [24] L. Pishchulin, M. Andriluka, P. Gehler, and B. Schiele. Poselet conditioned pictorial structures. In *CVPR*, 2013. [2](#)
- [25] L. Pishchulin, M. Andriluka, P. Gehler, and B. Schiele. Strong appearance and expressive spatial models for human pose estimation. In *ICCV*, 2013. [2](#)
- [26] V. Ramakrishna, D. Munoz, M. Hebert, J. A. Bagnell, and Y. Sheikh. Pose Machines: Articulated Pose Estimation via Inference Machines. In *ECCV*, 2014. [1, 2, 3, 6](#)
- [27] D. Ramanan, D. A. Forsyth, and A. Zisserman. Strike a Pose: Tracking people by finding stylized poses. In *CVPR*, 2005. [2](#)
- [28] S. Ross, D. Munoz, M. Hebert, and J. A. Bagnell. Learning message-passing inference machines for structured prediction. In *CVPR*, 2011. [2](#)
- [29] B. Sapp and B. Taskar. MODEC: Multimodal Decomposable Models for Human Pose Estimation. In *CVPR*, 2013. [4, 7](#)
- [30] L. Sigal and M. J. Black. Measure locally, reason globally: Occlusion-sensitive articulated pose estimation. In *CVPR*, 2006. [2](#)
- [31] K. Simonyan and A. Zisserman. Very deep convolutional networks for large-scale image recognition. *arXiv preprint arXiv:1409.1556*, 2014. [2](#)
- [32] M. Sun and S. Savarese. Articulated part-based model for joint object detection and pose estimation. In *ICCV*, 2011. [2](#)
- [33] C. Szegedy, W. Liu, Y. Jia, P. Sermanet, S. Reed, D. Anguelov, D. Erhan, V. Vanhoucke, and A. Rabinovich. Going deeper with convolutions. *arXiv preprint arXiv:1409.4842*, 2014. [1, 2](#)
- [34] Y. Tian, C. L. Zitnick, and S. G. Narasimhan. Exploring the spatial hierarchy of mixture models for human pose estimation. In *ECCV*, 2012. [2](#)
- [35] J. Tompson, R. Goroshin, A. Jain, Y. LeCun, and C. Bregler. Efficient object localization using convolutional networks. *CVPR*, 2015. [2, 7](#)
- [36] J. J. Tompson, A. Jain, Y. LeCun, and C. Bregler. Joint training of a convolutional network and a graphical model for human pose estimation. In *NIPS*, 2014. [2, 7](#)
- [37] A. Toshev and C. Szegedy. DeepPose: Human pose estimation via deep neural networks. *CVPR*, 2013. [2](#)
- [38] Z. Tu and X. Bai. Auto-context and its application to high-level vision tasks and 3d brain image segmentation. *IEEE Transactions on Pattern Analysis and Machine Intelligence*, 32(10):1744–1757, 2010. [2](#)
- [39] Y. Wang and G. Mori. Multiple tree models for occlusion and spatial constraints in human pose estimation. In *ECCV*, 2008. [2](#)
- [40] Y. Yang and D. Ramanan. Articulated pose estimation with flexible mixtures-of-parts. In *CVPR*, 2011. [2](#)
- [41] Y. Yang and D. Ramanan. Articulated human detection with flexible mixtures of parts. *TPAMI*, 2013. [7](#)